



# Highly efficient removal of Cr(VI) and Cu(II) by biochar derived from *Artemisia argyi* stem

Jiayang Song<sup>1</sup> · Qiulai He<sup>1</sup> · Xiaoling Hu<sup>1</sup> · Wei Zhang<sup>1</sup> · Chunyan Wang<sup>1</sup> · Rongfan Chen<sup>1</sup> · Hongyu Wang<sup>1</sup> · Ahmed Mosa<sup>2</sup>

Received: 2 January 2019 / Accepted: 13 March 2019 / Published online: 21 March 2019  
© Springer-Verlag GmbH Germany, part of Springer Nature 2019

## Abstract

In this work, a novel biochar was prepared from the *Artemisia argyi* stem at 300 °C (AS300), 450 °C (AS450), and 600 °C (AS600). The structural properties of these biochars were characterized with various tools. The sorption kinetic processes of Cr(VI) and Cu(II) onto these biochars were better described by the pseudo-second order. The sorption isotherm processes of Cr(VI) onto these biochars were better described by the Freundlich model while the adsorption processes of Cu(II) were consistent with the Langmuir model. Batch sorption experiments showed that AS600 had the maximum adsorption capacity to Cr(VI) and Cu(II) with 161.92 and 155.96 mg/g, respectively. AS600 was selected for the follow-up batch and dynamic adsorption experiments. Results showed that AS600 had larger adsorption capacity for Cr(VI) at lower pH while the larger adsorption capacity for Cu(II) was found at higher pH. The effect of ionic strength on the adsorption of Cu(II) by AS600 was greater than that on the adsorption of Cr(VI). Dynamic adsorption experiments showed that Cu(II) had a higher affinity for the adsorption sites on the AS600 compared with Cr(VI). The adsorption mechanisms mainly involved electrostatic attraction, ion exchange, pore filling, and chemical bonding effect.

**Keywords** Biochar · *Artemisia argyi* · Chromium · Copper · Adsorption · Dynamic adsorption

## Introduction

In recent years, heavy metal pollution is becoming one of the major environmental problems in the world (Rizwan et al. 2016). Once the heavy metals invade the human

body, they will gradually accumulate in certain organs in the body and cause chronic poisoning (Zhang et al. 2018a). Just as the excessive intake of Cr can cause headaches, nausea, diarrhea, vomiting, and other symptoms (An et al. 2018). Cu poisoning can seriously impair liver function and induce Wilson disease (Saber et al. 2018). There are many treatment methods for the removal and recovery of heavy metal pollution in water, such as chemical precipitation, coagulation, membrane separation, ion exchange, and electrolytic methods (Burakov et al. 2018; Fan et al. 2018). Compared with the high cost, high-energy requirements, sensitive operating conditions, and massive residual sludge of these methods, adsorption is considered to be an economical and effective choice for removing heavy metals from wastewater (Burakov et al. 2018; Fan et al. 2018; Hu et al. 2015). The choice of the adsorbents in the adsorption process is particularly important, and the currently used adsorbents may be of mineral, organic, or biological sources, such as activated carbon, zeolites, clay minerals, industrial by-products, agricultural waste, biomass, and polymeric materials (Burakov et al. 2018; Thines et al. 2017; Zhao et al. 2018b). At present,

## Highlights

- *Artemisia argyi* stem was firstly prepared into biochars for heavy metal removal.
- *Artemisia argyi* stem biochar had strong adsorption capacity to Cr(VI) and Cu(II).
- The maximum adsorption capacities were 161.92 and 155.96 mg/g, respectively.
- A new way of utilization was found for the *Artemisia argyi* stem.

Responsible editor: Tito Roberto Cadaval Jr

✉ Hongyu Wang  
hywang96@126.com

<sup>1</sup> School of Civil Engineering, Wuhan University, Wuhan 430072, China

<sup>2</sup> Soils Department, Faculty of Agriculture, Mansoura University, Mansoura 35516, Egypt

most of the traditional adsorbents used for the treatment of heavy metal pollution in the water body are physically or chemically activated. In practical applications, there are bottlenecks such as high cost and easy-to-cause secondary pollution. The biochar adsorbent prepared by the directly pyrolyzed biomass has the characteristics of eco-environmental protection, simple operation, wide adaptability, and no secondary pollution, which can make up for the deficiency of the traditional adsorbent (Essandoh et al. 2015).

Biochar, a class of carbon-rich, stable, and highly aromatic solid products, is derived from biomass pyrolysis at moderate or high temperature under anoxic or anaerobic conditions (Mohan et al. 2014). Biochar has large specific surface area and porosity, highly aromatization structure, and surface functional groups such as carboxyl group, hydroxyl group, and acid anhydride (Inyang et al. 2016). These surface structures make biochar have good adsorption properties. Currently, biomass-derived biochars have been used as effective adsorbents to remove heavy metals from aqueous solutions (Zhang et al. 2018c). Biochar is becoming a low-cost and economic substitution to activated carbon to remove multiple contaminants (Oliveira et al. 2017).

Biochar can be produced from a wide range of raw materials including natural plants, industrial and agricultural waste, municipal sludge, and livestock manure, such as sludge (Fan et al. 2019), wood (Zhang et al. 2018c), swine manure (Meng et al. 2014), microalgae (Saber et al. 2018), rice straw (Deng et al. 2018), crawfish shell (Yan et al. 2018), and other raw materials. The feedstock type and preparation conditions of biochar determine its physicochemical properties that would further influence its adsorption performance (Ahmad et al. 2014). These properties are mainly reflected in the pH, porosity and total pore volume, specific surface area, composition of compound and ash content, water holding capacity of materials, and so on. The cost and adsorption capacities are highly dependent on the properties of the biochars (Meng et al. 2014). For large-scale applications of biochar on wastewater treatment, it is meaningful to find a biomass with lower cost and higher adsorption capacity for preparing biochar.

*Artemisia argyi*, belonging to the genus *Artemisia* of the *Asteraceae*, is a perennial herb or a slightly semi-shrubby perennial herb with a strong aroma (Zhang et al. 2013). The *Artemisia argyi* contains plentiful flavonoids and is widely used in the food and pharmaceutical industries (Fu et al. 2018). Its leaves are widely used in clinical treatments (Liu et al. 2018; Yang et al. 2016), while the residual parts are always disposed, which makes pollution to the environment and is also a waste of natural resources. As a large planting country and a big consumer country of *Artemisia argyi*, China's *Artemisia argyi* planting area has exceeded 12,000 ha. In view of this, it is urgent to seek a resource

utilization route for *Artemisia argyi* stems (AAS). In previous studies, rapeseed stem (Zhao et al. 2018a), *Melia azedarach* wood (Zhang et al. 2018c), and maize straw (Li et al. 2018a) have been pyrolyzed into biochar, which have a good effect on the removal of contaminants. Considering that the AAS has similar properties to these substances and its wooden vascular structure is easy to form pore channels, it is appropriate to pyrolyze the AAS into biochar.

Besides the feedstock type, pyrolysis conditions, especially the pyrolysis temperature, also affect the properties of biochar via changing both the morphology structure and surface chemical functional groups (Zhang et al. 2017; Zhao et al. 2018a). Lee et al. (2013) prepared *Miscanthus* biochar and found that the specific surface area gradually increased as the pyrolysis temperature increased from 450 to 500 °C, which is beneficial for adsorbing contaminants. Zhao et al. (2018a) pyrolyzed rapeseed stem biochar under various temperatures (200–700 °C) and found that pyrolysis temperature is significantly correlated to biochar yield, fixed C and surface area. Due to changes in their physicochemical properties, biochars prepared at different pyrolysis temperatures (300, 450, and 600 °C) were observed to have significantly different adsorption capacities for heavy metals (Xiao et al. 2017). In order to optimize its adsorption capacity, it is necessary to find the optimum pyrolysis temperature for biochar preparation.

The adsorption process of heavy metal ions by biochar is affected by many factors, such as initial concentration, contact time, solution pH, and ionic strength (Burakov et al. 2018). The initial concentration and contact time can reflect the adsorption behavior and adsorption mechanism of biochar on heavy metals. This adsorption process can be described by isotherm models and kinetic models, respectively (Inyang et al. 2016). The pH can affect the charge distribution on the surface of the biochar and the existing form of heavy metal ions in solution (Wang et al. 2015). The ionic strength of the solution also plays an important role in the adsorption of heavy metals through its influence on the electrostatic double layer of biochar (Xiao et al. 2017). Previous studies have found that the coexistence of multiple heavy metal ions may reduce the adsorption capacity of biochar on heavy metal ions (Park et al. 2016).

Therefore, this study directly pyrolyzed the AAS into a novel biochar for the first time and conducted a series of experiments to evaluate the adsorption properties of *Artemisia argyi* stem biochar (ASB) for Cr(VI) and Cu(II) in aqueous solution. The objectives of this study were as follows: (1) prepare and characterize the ASB; (2) study the effects of pyrolysis temperatures, pH, ionic strength, and coexisting ions on the adsorption of heavy metals by the ASB; and (3) understand the responsible mechanisms of the adsorption processes. This work might add some new insights into the concept of natural waste disposal and recycling.

## Materials and methods

### Materials

All of the reagents and chemicals used in this study were of analytical grade, and the solutions were all prepared using deionized (DI) water. Potassium bichromate ( $K_2Cr_2O_7$ ), copper nitrate trihydrate ( $Cu(NO_3)_2 \cdot 3H_2O$ ), nitric acid ( $HNO_3$ ), sodium hydroxide (NaOH), and sodium chloride (NaCl) were purchased from Sinopharm Chemical Reagent Co., Ltd., China. AAS were collected from a company in Nanyang producing *Artemisia* products (Henan Province, China).

### Biochar production

The raw materials were washed repeatedly with deionized water until the surface impurities were cleaned up, and then the surface was repeatedly washed again with DI water until neutral. It was dried in an oven to a constant weight and placed in an airtight container prior to use.

AAS were pyrolyzed in a tube furnace under  $N_2$  flow at different temperatures (300, 450, and 600 °C) for 2 h. The obtained biochar was repeatedly washed again with DI water until neutral and oven dried at 105 °C. The biochar samples were ground and pulverized using a mortar and sieved to form a homogeneous biochar (0.9–1.0 mm). The samples were labeled as AS300, AS450, and AS600, respectively, and then placed in a dry airtight container for later use.

### Biochar characterization

The contents of organic elements C, H, and N in the biochar were analyzed by a CHN elemental analyzer (RARIO EL III, Elementar, Germany). The ash content was calculated by the mass difference method (Keiluweit et al. 2010; Li et al. 2018a). The content of the O element was obtained by subtracting the contents of C, H, N, and ash in the total mass of the sample (Li et al. 2018a). The yield was calculated by the mass ratio of the biochar to the biomass feedstock. The specific surface area and pore size distribution were measured by a multi-channel-specific surface area and pore size analyzer (TriStarII3020, Micromeritics, USA) using the Brunauer-Emmett-Teller (BET) method. The surface morphology of the biochar was measured by a scanning electron microscope (SEM, JEM-6700F, Japan). The surface functional groups were qualitatively analyzed using a Fourier transform infrared spectroscopy (FTIR, Thermo Nicolet, 6700, Madison, WI, USA). The changes of crystalline elements in the biochar before and after adsorption were characterized by an X-ray Diffractometer (XRD, D8 Advance, BRUKER AXS GMBH, Germany) operated at 40 kV and 40 mA using  $Cu K_{\alpha}$  radiation (Zhang et al. 2018b).

### Sorption experiments

Of a certain mass concentration, 0.1 g biochar and 50 mL heavy metal solution were mixed in a 250 mL conical flask. The flask was sealed with a plastic film and shaken with a speed of 120 r/min for a certain period of time at  $25 \pm 0.5$  °C in a gas bath thermostat. The concentration of heavy metals in the filtrate was determined by an inductively coupled plasma-atomic emission spectrometry (ICP-OES, Optima 4300DV, PerkinElmer SCIEX, USA) after the suspension was filtered with a 0.45  $\mu m$  microfiltration membrane. All experiments were performed in triplicates. The adsorption amounts of Cr(VI) and Cu(II) on different biochars were calculated as follows:

$$q_e = \frac{V(C_0 - C_e)}{m} \quad (1)$$

where  $q_e$  is the adsorption amount of the adsorbent at equilibrium (mg/g),  $C_0$  is the initial solution concentration (mg/L),  $C_e$  is the adsorption equilibrium solution concentration (mg/L),  $V$  is the solution volume (L), and  $m$  is the amount of biochar (g).

### Sorption kinetics

The initial mass concentrations of Cr(VI) and Cu(II) solutions were both 50 mg/L, and the adsorption time was set to 5, 10, 20, 30, 60, 120, 300, 600, 900, 1440, and 2880 min. The variation of the adsorption capacity with time was described using a dynamic curve. In order to clarify the reaction order and adsorption mechanism of the adsorption process, the adsorption kinetic data were fitted by pseudo-first-order, pseudo-second-order, and Elovich models. The governing equations of these kinetic models are as follows:

$$\text{Pseudo-first-order : } q_t = q_e(1 - \exp(-k_1 t)) \quad (2)$$

$$\text{Pseudo-second-order : } q_t = \frac{k_2 q_e^2 t}{1 + k_2 q_e t} \quad (3)$$

$$\text{Elovich : } q_t = \frac{1}{\beta} \ln(\alpha \beta t + 1) \quad (4)$$

where  $q_t$  and  $q_e$  are the adsorption amount of the adsorbent at time  $t$  and equilibrium (mg/g), respectively,  $k_1$  and  $k_2$  are the pseudo-first- and pseudo-second-order apparent adsorption rate constants ( $h^{-1}$ ), respectively,  $\alpha$  is the initial adsorption rate (mg/kg), and  $\beta$  is the desorption constant (kg/mg).

### Sorption isotherms

The initial mass concentration gradients of Cr(VI) and Cu(II) solutions were set to 4, 10, 20, 30, 40, 60, 80, 120, and

**Table 1** Bulk element composition, ash content, and atomic ratio of ASB

Biochar	Bulk element composition and ash contents (%)					Bulk atomic ratio		
	C	H	N	O	Ash	(N + O)/C	O/C	H/C
AS300	69.22	4.63	0.73	21.94	3.48	0.328	0.317	0.067
AS450	77.03	3.28	0.63	13.74	5.32	0.187	0.178	0.043
AS600	84.32	2.11	0.40	6.50	6.68	0.082	0.077	0.025

(N + O)/C, atomic ratio of sum of N and O to C, the higher value indicates the greater polarity; O/C, atomic ratio of O to C, the higher value indicates the greater polarity; H/C, atomic ratio of H to C, the lower value indicates the higher aromaticity

160 mg/L, and the contact time was 24 h. In order to better study the adsorption behavior of the adsorbent, the isotherm adsorption data were fitted by the Langmuir model and the Freundlich model. The governing equations of these kinetic models are as follows:

$$\text{Langmuir sorption isotherm : } q_e = \frac{KS_{\max}C_e}{1 + KC_e} \quad (5)$$

$$\text{Freundlich isotherm adsorption : } q_e = K_f C_e^n \quad (6)$$

where  $K$  and  $K_f$  represent the Langmuir bonding term related to interaction energies (L/mg) and the Freundlich affinity coefficient ( $\text{mg}^{(1-n)}\text{L}^n/\text{g}$ ), respectively,  $S_{\max}$  denotes the Langmuir maximum capacity (mg/g), and  $n$  is the Freundlich linearity constant.

Some of the adsorbed adsorbents were rinsed with DI water, dried in an oven at 105 °C, and then stored for further characterization tests. The biochar with the maximum adsorption capacity for Cr(VI) and Cu(II) in the preliminary evaluation test was selected for the follow-up tests.

### Effects of pH and ionic strength

The initial mass concentrations of Cr(VI) and Cu(II) solutions were both 100 mg/L. In order to study the effects of the initial pH and ionic strength of solution on the adsorption of Cr(VI) and Cu(II), the initial pH of Cr(VI) and Cu(II) solution were

set to 1.0–10.0 and 1.0–7.0, respectively. The NaCl concentration in the solution ranged from 0 to 0.5 mol/L. The concentration of heavy metals in the filtrate was determined by ICP after shaking at  $25 \pm 0.5$  °C for 24 h. The pH of the solution was adjusted with NaOH or HNO<sub>3</sub> solutions (1.0 mol/L).

### Dynamic sorption experiments

A mixed solution in which both Cr(VI) and Cu(II) concentrations were 100 mg/L was prepared. In triplicate, biochar (3 g) was loaded into an adsorption column ( $D \times H = 16 \text{ mm} \times 240 \text{ mm}$ ). The above mixed solution of Cr(VI) and Cu(II) was flowed through the adsorption column at a flow rate of 20 mL/h using a peristaltic pump. The effluent samples were collected at the top of the column by the operation mode of the bottom-in and upper-out, and the dynamic adsorption efficiency was studied according to the concentration variation of Cr(VI) and Cu(II) in the effluent. Concentrations of Cr(VI) and Cu(II) in the effluent were determined by ICP.

## Results and discussion

### Effect of pyrolysis temperature on physicochemical properties of biochars

The pyrolysis temperature had a significant effect on the elemental composition of biochar (Xiao et al. 2017). The ash

**Table 2** The yields and BET characteristics of ASB

Biochar	Yield (%)	BET surface area (m <sup>2</sup> /g)	t-plot micropore area (m <sup>2</sup> /g)	BJH adsorption cumulative surface area (m <sup>2</sup> /g)	Single-point adsorption total pore volume (cm <sup>3</sup> /g)	BJH adsorption cumulative volume (cm <sup>3</sup> /g)	t-plot micropore volume (cm <sup>3</sup> /g)	BJH adsorption average pore width (nm)
AS300	38.96	1.85	0.85	0.21	$1.87 \times 10^{-3}$	$1.62 \times 10^{-3}$	$4.31 \times 10^{-4}$	31.08
AS450	28.98	56.99	30.16	8.65	$2.44 \times 10^{-2}$	$9.43 \times 10^{-3}$	$1.56 \times 10^{-2}$	4.36
AS600	25.68	81.57	44.10	11.10	$3.12 \times 10^{-2}$	$8.90 \times 10^{-3}$	$2.28 \times 10^{-2}$	3.21

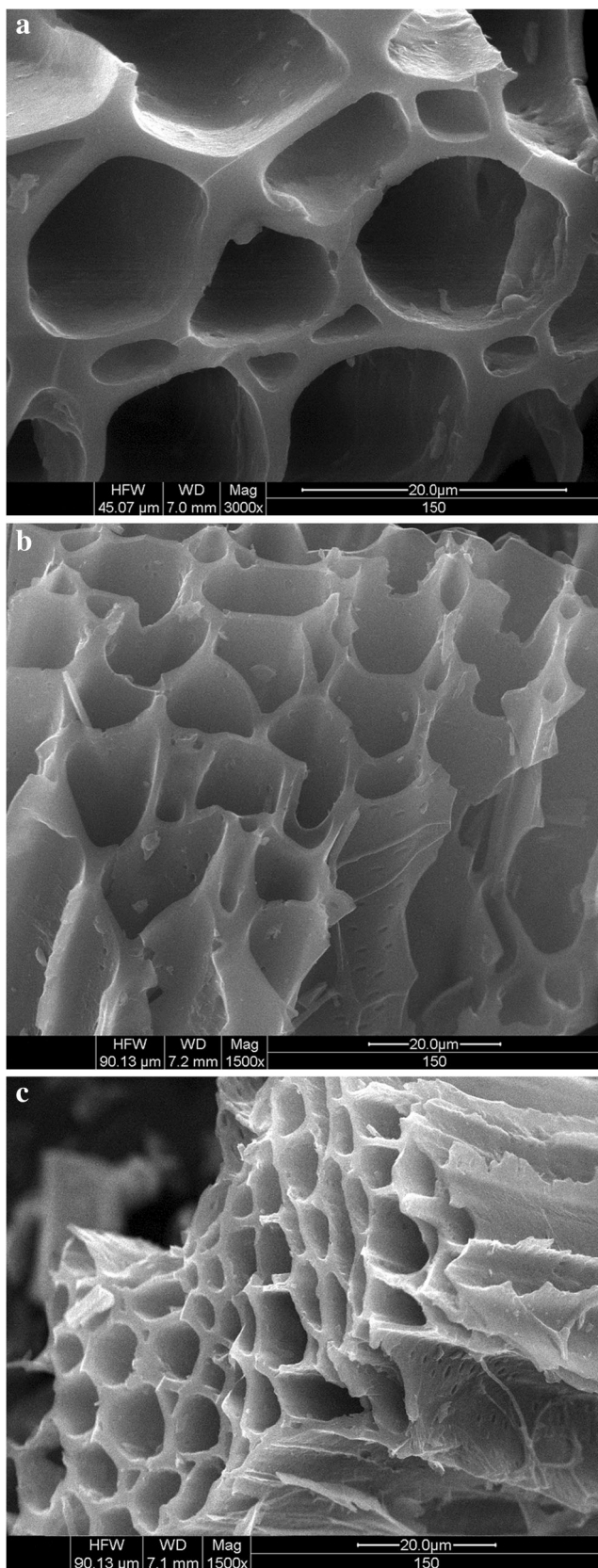


Fig. 1 The SEM images of a AS300, b AS450, and c AS600

content of pyrolytic biochar at high temperature was higher than that of pyrolytic biochar at low temperature, which was expressed as AS600 > AS450 > AS300 (Table 1). The ash content in biochar was mainly related to the metal elements, carbonates, and silicates contained in the biomass raw materials. As the pyrolysis temperature increased, organic matter and volatile substances decreased and non-volatile substances such as oxides and silicates remained in biochar, causing the relative content of ash to rise (Chow et al. 2004).

The proportion of each element in biochar varied with the pyrolysis temperature. The highest content in the three biochars was C element, followed by O element, while the contents of H and N were relatively low (Table 1). The content of C increased with the rising of pyrolysis temperature, which meant that the degree of carbonization of the biomass became more obvious at higher temperature. This could be because the decomposable organic carbon in the AAS had been completely pyrolyzed at a lower pyrolysis temperature, while the fixed carbon continued to carbonize and concentrate instead of decomposing and reducing at the higher pyrolysis temperature (Bruun et al. 2011). Under high-temperature conditions, the contents of H, N, O, and other elements in biochar were lowered because the high pyrolysis temperature caused the decomposition of organic matter and the decrease of groups such as hydroxyl groups, carboxyl groups, and carbonyl groups attached to carbon (Cantrell et al. 2012). The atomic ratio of (N + O)/C and O/C can characterize the polarity of biochar, and H/C was an indicator of the aromaticity of biochar (Chefetz and Xing 2009). The aromaticity of the three biochars was expressed as AS600 > AS450 > AS300, which indicated that the volatile organic matter in AAS disappeared and more amorphous carbon can be converted into condensed aromatic carbon with the increase of pyrolysis temperature (Li et al. 2018a). The polarity of biochar decreased with the temperature, which may be due to the breakage of groups such as

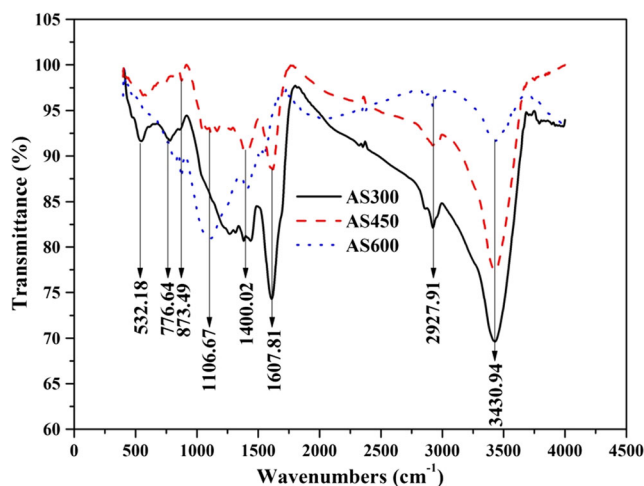
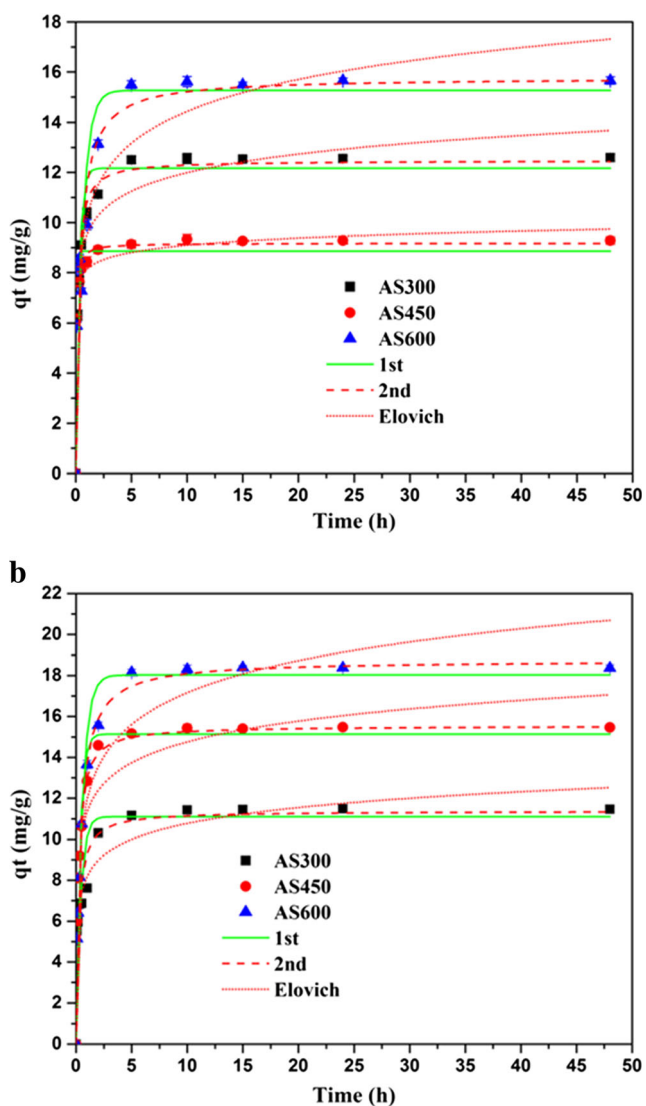


Fig. 2 FTIR spectra of AS300, AS450, and AS600



**Fig. 3** Sorption kinetics data and fitted models of heavy metal ions onto the ASB: **a** Cr(VI) and **b** Cu(II)

amino (-NH<sub>2</sub>), hydroxyl (-OH), and carboxyl (-COOH) linked to carbon skeleton in biochar (Uchimiya et al. 2011).

The yields of ASB gradually decreased with the temperature (Table 2). This was because the volatile components in biomass were gradually escaping from the raw materials when the pyrolysis temperature rose, which made the residual mass less and less. The yields of the ASB were 25.68% to 38.96%, which was slightly lower than the average yields of biochars produced from other feedstocks reported, such as rice straw, algal, and livestock and poultry manure (Li et al. 2018b; Yu et al. 2017). There are many factors that significantly affect the yield of biochar produced via pyrolysis, mainly including pyrolysis temperature, pyrolysis type, residence time, and feedstock properties (Tripathi et al. 2016). In this study, the reason for the lower yields of washed AAS may be attributed to the loss of hydrocarbon moieties capable of promoting cross-

linking reactions that foster char production (Cantrell et al. 2012).

The specific surface area and pore size structure of biochar can explain its adsorption capacities to heavy metals (Peng et al. 2016). The BET surface area, micropore area, single-point total pore volume, and micropore volume of biochar increased with the rising of pyrolysis temperature, which indicated that the structural characteristics of biochar had a great dependence on the pyrolysis temperature (Table 2). At lower temperatures, incomplete carbonization can make most of the amorphous carbon stay on the biochar, which may hinder the pore structure and reduce the BET surface area and porosity. However, higher temperatures result in higher carbonization, conversion of amorphous carbon to higher density aromatic carbons, and removal of aliphatic volatiles to form more pores (Keiluweit et al. 2010). The micropore areas of AS600, AS450, and AS300 accounted for 54.06, 52.92, and 45.95% of the BET-specific surface area, respectively, indicating that the biochar derived from the AAS was prone to form a microporous structure. Previous studies had shown that the micropores of biochar were mainly caused by aromatic structures rather than aliphatic structures (Han et al. 2014). In this study, with the rising of temperature, the aromaticity of biochar and the proportion of micropore volume in the total pore volume increased, while the average pore width of biochar decreased, which further indicated that a large number of mesopore and micropore structures were formed on the surface of the ASB at higher temperature.

Comparing the SEM images of AS300, AS450, and AS600 (Fig. 1), it was found that the surface fiber structure of ASB was smooth and fine, and its internal hierarchical structure was distinct. There were a large number of pores and channels, which not only strengthened the contact between the adsorption sites on the surface of biochar and heavy metal ions but also helped to the introduction of new functional groups. With the increase of pyrolysis temperature, the micropore structure began to form on the surface of the biochar, which can increase the specific surface area of the biochar and reduce the average pore size of the biochar. That was consistent with the results obtained in Table 2. Therefore, as an adsorbent, ASB had certain structural advantages, which will contribute to enhance the physical adsorption capacities.

It can be seen from the FTIR spectra (Fig. 2) that the number of functional groups on the surface of the ASB gradually decreased at higher temperature. These changes were mainly reflected in the bending vibration of C–H in olefins and aromatics (625–1000 cm<sup>-1</sup>), the stretching vibration level 2 of C–O in hydroxyl (1070–1120 cm<sup>-1</sup>), the bending vibration of O–H/C–H in olefins, alkyds, phenols and alcohol (1360–1430 cm<sup>-1</sup>), the stretching vibration of C=C in Aromatic structures (1450–1610 cm<sup>-1</sup>), the stretching vibration of C–H in fatty chain structure (2700–3000 cm<sup>-1</sup>), and the stretching vibration of O–H in hydroxyl (3200–3700 cm<sup>-1</sup>)

**Table 3** Best-fit parameters for kinetic models of heavy metal sorption onto the ASB

Adsorbate	Biochar	Kinetic models	Parameter 1	Parameter 2	R <sup>2</sup>
Cr(VI)	AS300	Pseudo-first-order	$k_1 = 3.4148$	$q_e = 12.1686$	0.9361
		Pseudo-second-order	$k_2 = 0.5261$	$q_e = 12.4798$	0.9786
		Elovich	$\alpha = 7961.45$	$\beta = 0.9353$	0.9762
	AS450	Pseudo-first-order	$k_1 = 12.9970$	$q_e = 8.8607$	0.9731
		Pseudo-second-order	$k_2 = 2.3683$	$q_e = 9.1737$	0.9951
		Elovich	$\alpha = 1.5867$	$\beta = 2.4277$	0.9871
	AS600	Pseudo-first-order	$k_1 = 1.6470$	$q_e = 15.2671$	0.9072
		Pseudo-second-order	$k_2 = 0.1713$	$q_e = 15.7743$	0.9528
		Elovich	$\alpha = 486.49$	$\beta = 0.5462$	0.9461
Cu(II)	AS300	Pseudo-first-order	$k_1 = 2.4783$	$q_e = 11.1021$	0.8991
		Pseudo-second-order	$k_2 = 0.4030$	$q_e = 11.3803$	0.9711
		Elovich	$\alpha = 1720.34$	$\beta = 0.8953$	0.9544
	AS450	Pseudo-first-order	$k_1 = 2.8786$	$q_e = 15.1422$	0.9648
		Pseudo-second-order	$k_2 = 0.3337$	$q_e = 15.551$	0.9913
		Elovich	$\alpha = 3410.73$	$\beta = 0.6813$	0.9631
	AS600	Pseudo-first-order	$k_1 = 1.8413$	$q_e = 18.0305$	0.9778
		Pseudo-second-order	$k_2 = 0.1485$	$q_e = 18.7411$	0.9935
		Elovich	$\alpha = 461.621$	$\beta = 0.4443$	0.9605

$\alpha$ , the initial adsorption rate (mg/kg);  $\beta$ , the desorption constant (kg/mg);  $q_e$ , the amount of adsorbate in the adsorbent at equilibrium (mg/g);  $k_1$ , the pseudo-first-order apparent adsorption rate constant ( $h^{-1}$ );  $k_2$  the pseudo-second-order ( $h^{-1}$ );  $R^2$ , the correlation coefficient values

(Xiao et al. 2017). The changes of these functional groups revealed the dehydration and molecular transformation of biomass during pyrolysis process (Yao et al. 2011). This indicated that there are a large number of oxygen-containing functional groups in the ASB. As a low-cost adsorbent, ASB has great potential for application.

### Sorption experiments

#### Sorption kinetics

The adsorption capacity of Cr(VI) and Cu(II) onto the ASB was gradually accumulated with time, and then remained stable at a certain level (Fig. 3). For all the metal ions tested, about 80% of the adsorption occurred within the first few hours, then the adsorption rate decreased, and the adsorption gradually reached equilibrium after 10 h. This was because at the initial stage of adsorption, the porous channels and functional groups on the surface of adsorbent were abundant, which can provide more binding sites, and be more favorable for the adsorption of heavy metal ions. As the adsorption continued, the reduction of active binding sites and the enhancement of the electrostatic repulsion between ions made it difficult for the adsorption reaction to continue, thus achieved adsorption equilibrium (Lu et al. 2012).

In order to study the rate-limiting steps in the adsorption process, the adsorption kinetic data were fitted and analyzed using the pseudo-first-order, pseudo-second-order, and Elovich models (Fig. 3). The correlation coefficient values of the fitting results of the pseudo-second-order kinetic model for the adsorption of Cr(VI) and Cu(II) on the ASB were

higher than that of the other two models (Table 3), and the measured equilibrium adsorption amounts were also closer to the equilibrium adsorption amounts calculated by the pseudo-second-order kinetic equation. These results indicated that the pseudo-second-order kinetic model was more suitable to describe the adsorption process of Cr(VI) and Cu(II) onto the ASB. The pseudo-second-order kinetic model can reflect the adsorption kinetics mechanism of liquid–solid reaction more comprehensively (Fang et al. 2014), such as external liquid membrane diffusion, surface adsorption, and intra-particle diffusion, which can more accurately reflect the adsorption process of Cr(VI) and Cu(II) onto the ASB.

#### Sorption isotherms

With the increase of initial concentration of heavy metal ions, the adsorption capacities of Cr(VI) and Cu(II) on the ASB increased rapidly and then gradually stabilized (Fig. 4). The adsorption capacities of three biochars to Cr(VI) and Cu(II) were AS600 > AS300 > AS450, and AS600 > AS450 > AS300, respectively (Table 4). The maximum adsorption capacities of AS600 to Cr(VI) and Cu(II) were 161.92 and 155.96 mg/g, respectively.

In order to further study the isothermal adsorption characteristics of heavy metal ions on the ASB, the isotherm adsorption data of Cr(VI) and Cu(II) adsorbed by the ASB were fitted by the Langmuir and Freundlich models (Fig. 4). For the adsorption process of Cr(VI), the fitting correlation coefficient values of Freundlich model were better than that of the Langmuir model (Table 4). Therefore, the Freundlich model was more suitable to describe the adsorption process of Cr(VI)

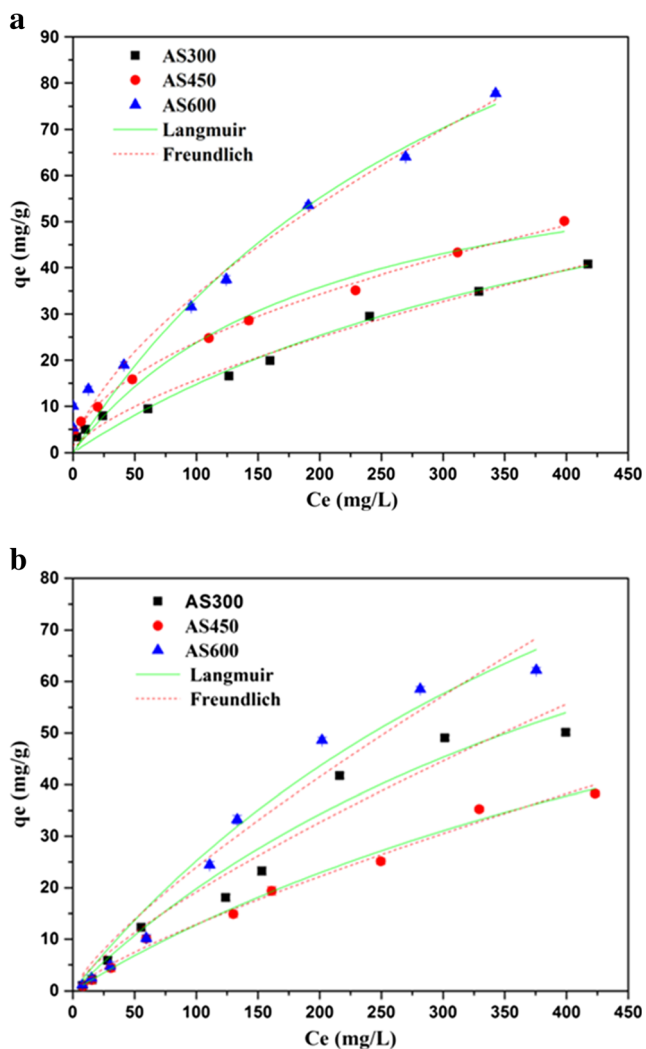


**Fig. 4** Sorption isotherm data and fitted models of heavy metal ions onto the ASB: **a** Cr(VI) and **b** Cu(II)

by the ASB. It also showed that the adsorption process of Cr(VI) was multi-molecular layer adsorption, which may be related to the functional groups carried on the surface of the ASB, such as hydroxyl (-OH) and carboxyl (-COOH). For the adsorption process of Cu(II), the correlation coefficient values of the Langmuir model were better than that of the Freundlich model, which indicated that the adsorption process of Cu(II) was monolayer adsorption and consistent with the Langmuir model. Compared with the maximum adsorption capacities of Cr(VI) and Cu(II) on the other adsorbents in the previous studies, ASB used in this study showed better adsorption performance (Table 5), which indicated that the AAS could be a highly efficient material for preparing biosorbent. Additionally, the raw materials are very cheap and easily available. Therefore, the ASB has attractive advantages such as simple production process, low cost and good adsorption capacity and had great potential for large-scale wastewater treatment.

## Effects of pH and ionic strength

The change of initial solution pH had a significant effect on the adsorption of heavy metals on ASB (Fig. 5). In the adsorption process, pH not only affected the surface properties of the adsorbents but also determined the forms of metal ions in solution (Wang et al. 2015). With the increase of pH, the adsorption capacity of Cr(VI) by AS600 decreased gradually and then tended to remain stable. The major reason for higher adsorption capacity of Cr(VI) at lower pH was that the carboxyl and hydroxyl groups on the surface of ASB can be protonated with hydrogen ions under the acidic environment, forming positive functional groups  $-OH_2^+$  and  $-COOH_2^+$ , which can be combined with the anions  $HCrO_4^-$  and  $Cr_2O_7^{2-}$  in the solution by electrostatic interaction (Shen et al. 2012). When the pH increased, the existing form of chromium changed from  $Cr_2O_7^{2-}$  to  $CrO_4^{2-}$  and the space occupied by a single chromium increased, moreover,  $OH^-$  can compete with  $HCrO_4^-$ ,  $Cr_2O_7^{2-}$  and  $CrO_4^{2-}$  for adsorption sites, all of which may result in the decrease of adsorption capacity (Wang et al. 2012). The adsorption of Cu(II) by AS600 was also significantly affected by the initial pH of the solution (Fig. 5). The adsorption capacity of Cu(II) increased with the variation of pH from 1.0 to 7.0. This was mainly due to the influence of pH on the existing forms of copper in the solution. When  $pH < 5.0$ , Cu(II) was the main existing form. In this case, a large number of  $H^+$  competed with Cu(II) for the limited binding sites on the surface of biochar, so the adsorption capacity was relatively little (Zhang et al. 2018a). When  $pH \geq 5.0$ , the content of  $[Cu(OH)]^+$  was the highest and the decrease of  $H^+$  weakened the repulsion of positive charges. Cu(II) in the solution was adsorbed in the form of its monovalent hydrolytate. With the increase of pH, the surface of biochar gradually turned into electronegativity, which enhanced the electrostatic attraction to free Cu(II). In addition, at high pH,  $Cu(OH)_2$  started to form and the adsorption capacity increased sharply. When the pH increased sequentially and exceeded 7.0, Cu(II) completely existed in the form of insoluble hydroxide precipitation. Previous studies had also shown that precipitation played an important role in the removal of heavy metal ions from aqueous solutions by biochar (Saber et al. 2018).

During the adsorption process, the ions generated by the hydrolysis of salt substances may compete with metal ions for adsorption sites to reduce the adsorption efficiency, or accelerate the effective collision between the adsorbents and the metal ions to increase the adsorption efficiency (Wang et al. 2015). As the Fig. 6 showed, the low concentration of NaCl ( $\leq 0.05$  mol/L) had little effect on the adsorption of Cr(VI) and Cu(II). However, when the concentration of NaCl was above 0.5 mol/L, the negative effect of ionic strength on the



**Table 4** Best-fit parameters for isotherm models of heavy metal sorption onto the ASB

Adsorbate	Biochar	Isotherm models	Parameter 1	Parameter 2	R <sup>2</sup>
Cr(VI)	AS300	Langmuir	$K = 0.0018$	$S_{max} = 127.66$	0.9767
		Freundlich	$K_f = 0.5561$	$n = 0.7687$	0.9885
	AS450	Langmuir	$K = 0.0013$	$S_{max} = 108.74$	0.9640
		Freundlich	$K_f = 0.3435$	$n = 0.7864$	0.9901
	AS600	Langmuir	$K = 0.0018$	$S_{max} = 161.92$	0.9714
		Freundlich	$K_f = 0.6219$	$n = 0.7929$	0.9893
Cu(II)	AS300	Langmuir	$K = 0.0020$	$S_{max} = 72.31$	0.9660
		Freundlich	$K_f = 0.7374$	$n = 0.6648$	0.9540
	AS450	Langmuir	$K = 0.0049$	$S_{max} = 89.06$	0.9911
		Freundlich	$K_f = 2.7182$	$n = 0.5202$	0.9884
	AS600	Langmuir	$K = 0.0027$	$S_{max} = 155.96$	0.9781
		Freundlich	$K_f = 1.7101$	$n = 0.6509$	0.9635

*K*, the Langmuir bonding term related to interaction energies (L/mg); *K<sub>f</sub>*, the Freundlich affinity coefficient (mg<sup>(1-n)</sup>L<sup>n</sup>/g); *S<sub>max</sub>*, the Langmuir maximum capacity (mg/g); *n*, the Freundlich linearity constant

adsorption of Cu(II) was more serious than that of Cr(VI). The main reasons for the above phenomenon were as follows: (1) At lower concentrations, the competitive ability of Cl<sup>-</sup> and Na<sup>+</sup> with metal ions to the adsorption sites on the adsorbent was weak and can be neglected. (2) When the Cl<sup>-</sup> and Na<sup>+</sup> in the solution reached a certain concentration, the existence of them would hinder the electrostatic attraction between the metal ions and the adsorbents, and compete with the metal ions for the adsorption sites. (3) High concentration of NaCl could increase the ionic strength of the solution, which could weaken the activity of the metal ions and result in a reduction of effective collision between the metal ions and the adsorbents (Xiao et al. 2017).

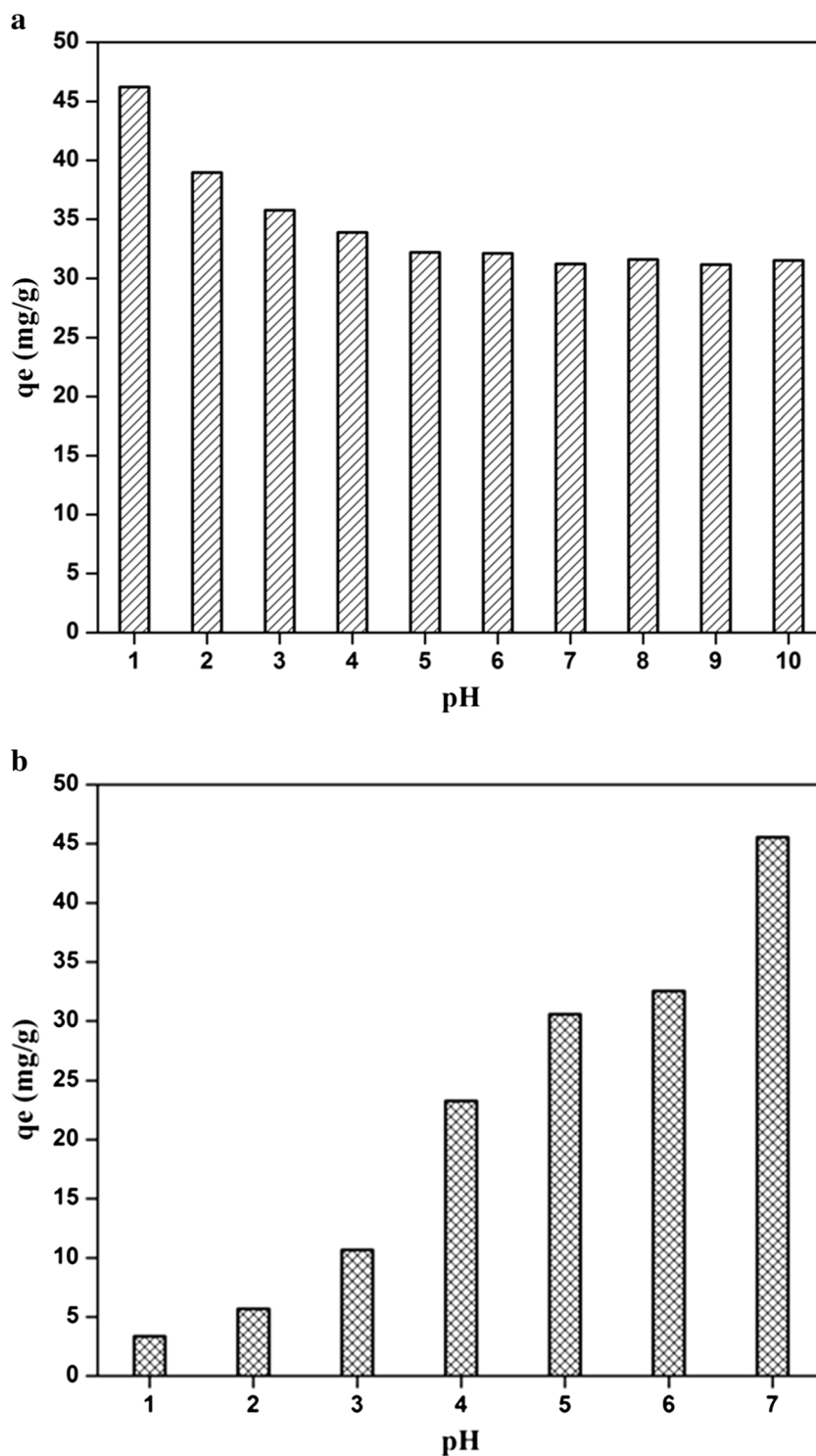
### Dynamic sorption experiments

The results of dynamic adsorption experiments were shown in Fig. 7. The removal rate of heavy metals increased at the initial stage of adsorption (< 1 h) and reached a peak at 1 h. The adsorption order was Cu(II) > Cr(VI). The removal rates of Cr(VI) and Cu(II) showed different degrees of decline after 2 h. Cr(VI) showed significant release at 4 h, while Cu(II) showed significant release at 6 h. This may be due to the interaction between metal ions in the mixed system. Cr(VI) in the mixed solution was mostly adsorbed to the surface of biochar in the form of HCrO<sub>4</sub><sup>-</sup>, and HCrO<sub>4</sub><sup>-</sup> usually had a large ionic space volume. With the reaction proceeding, more

**Table 5** Comparison of the maximum adsorption capacities of Cr(VI) and Cu(II) on the different adsorbents

Adsorbate	Adsorbent	Adsorption capacity (mg/g)	Reference
Cr(VI)	Clarified sludge	26.31	Kyzas and Kostoglou (2014)
	Fe <sup>0</sup> /Fe <sub>3</sub> O <sub>4</sub> nanoparticles	55.64	Rao et al. (2013)
	Magnetized activated carbon	57.19	Nethaji et al. (2013)
	Zinc–biochar nanocomposites	102.66	Gan et al. (2015)
	<i>Melia azedarach</i> wood magnetic biochar	25.27	Zhang et al. (2018c)
	AS600	161.92	This study
Cu(II)	<i>Spartina alterniflora</i> biochar	48.49	Li et al. (2013)
	Cortex banana waste	36	Kelly-Vargas et al. (2012)
	Swine manure biochar	21.94	Meng et al. (2014)
	Chestnut bur	34.77	Kim et al. (2015)
	Rice straw hydrochars	144.9	Li et al. (2018b)
	Ferromanganese binary oxide–biochar composites	64.9	Zhou et al. (2018)
	AS600	155.96	This study

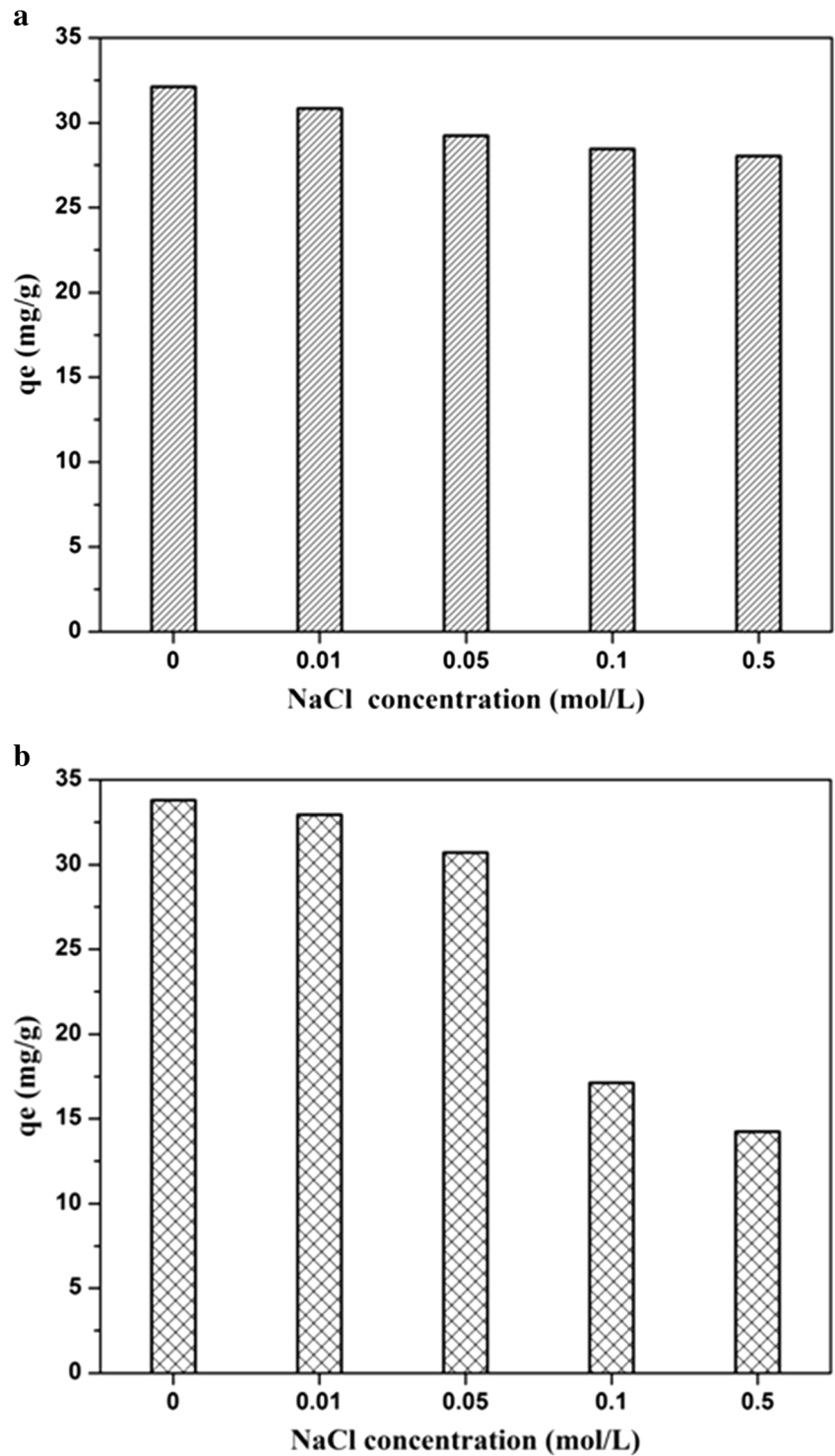
**Fig. 5** Effect of initial pH on heavy metal adsorption onto the ASB: **a** Cr(VI) and **b** Cu(II)



and more  $\text{HCrO}_4^-$  were adsorbed on the surface of AS600, thus forming a larger and larger ionic framework space near the surface of the AS600. The negatively charged framework structure and the free Cu(II) in solution were attracted to each other, so the adsorption effect on Cu(II) was better. The

adsorption sites on the AS600 were gradually saturated with time. Due to AS600 exhibited different dynamic adsorption capacities for Cr(VI) and Cu(II), Cr(VI), and Cu(II) had different degrees of release in solution, which was consistent with research results reported by Xiao et al. (Xiao et al. 2017).

**Fig. 6** Effect of solution ionic strength on heavy metal adsorption onto the ASB: **a** Cr(VI) and **b** Cu(II)

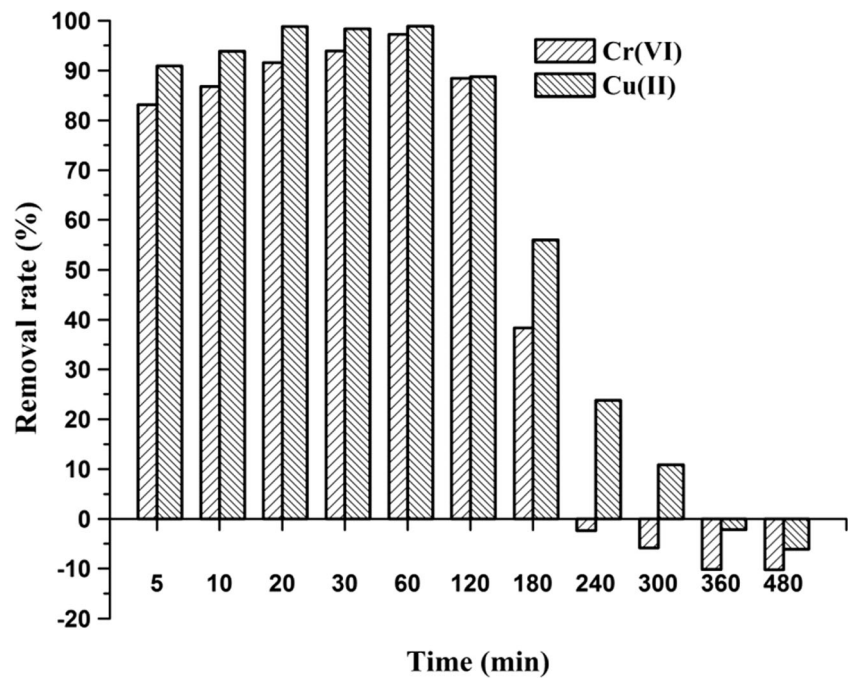


**Sorption mechanisms**

The XRD spectra (Fig. 8) showed that the surface structure of AS600 did not change significantly before and after adsorption of heavy metals, and there was no trace of

precipitate, indicating that the precipitation was not an important mechanism for the adsorption of Cr(VI) and Cu(II) by the ASB. The rapid initial adsorption phase observed in the adsorption kinetics and adsorption isotherm confirmed the participation of the physical adsorption mechanism, and

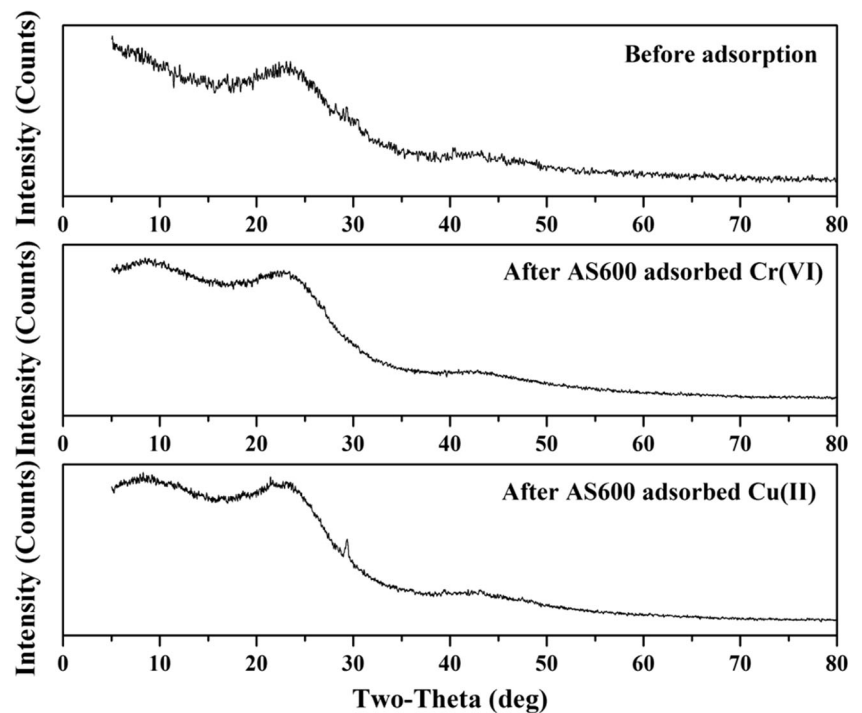
**Fig. 7** Dynamic adsorption experiments of heavy metal ions onto the ASB



the heavy metal ions entered the confirmed pores through the diffusion motion. Generally, the pH mainly affected the electrostatic action of the outer layer, and had little effect on the chemical bond of the inner layer. In the pH influence experiment, the adsorption capacity changed with the variation of pH, which could be understood as the influence of the adsorption of the outer layer by the pH.

Therefore, the existence of electrostatic attraction was concluded. If the adsorption of Cr(VI) and Cu(II) was caused only by electrostatic attraction, when the pH of counteracted the positive and negative charges on the surface of the ASB, there should be a low value inflection point. However, no such results were found in the experiment, so it could be inferred that in addition to the

**Fig. 8** XRD diffraction patterns before and after AS600 adsorption



electrostatic attraction effect, the chemical bond force also promoted the adsorption of heavy metals by the ASB, which led to the formation of the inner layer complex. The FTIR spectra showed the presence of hydroxyl, lactone, and carboxyl groups on the surface of the biochar. The distribution of a large number of oxygen-containing functional groups provided a good condition for the chemical complexation of Cr(VI) and Cu(II) on the biochar. A large amount of heavy metal ions were adsorbed to the surface of the ASB through the ion exchange and chemical bonding effects formed with hydroxyl, lactone, and carboxyl. This was the main chemical adsorption mode for removing heavy metal ions by the ASB.

## Conclusions

Batch and dynamic adsorption experiments were conducted to reveal the effects of pyrolysis temperature, pH, ionic strength, and coexisting ions on the adsorption of heavy metal ions by the ASB. The BET-specific surface area and the micropore area increased with the pyrolysis temperature, and a large number of mesopore and micropore structures occurred, thus achieving the maximum adsorption capacity of 161.92 and 155.96 mg/g for Cr(VI) and Cu(II) by AS600, respectively. The adsorption kinetic experiments showed that pseudo-second order was more suitable to describe the adsorption process of Cr(VI) and Cu(II) onto the ASB. The adsorption isotherm experiments showed that the Freundlich model was more suitable to describe the adsorption process of Cr(VI) by the ASB while the adsorption process of Cu(II) was consistent with the Langmuir model. The ASB had larger adsorption capacity for Cr(VI) at lower pH while the larger adsorption capacity for Cu(II) was found at higher pH. The ionic strength had a great influence on the adsorption of Cu(II) by the ASB and had little effect on the adsorption of Cr(VI). When Cr(VI) and Cu(II) coexisted, the ASB was more likely to adsorb Cu(II). This study confirmed that the ASB can be used as a low-cost and highly efficient adsorbent, providing a new way for its resource utilization.

**Acknowledgments** The authors also thank the anonymous reviewers for their invaluable insight and helpful suggestions.

**Funding information** This work was financially supported by the CRSRI Open Research Program (Program SN CKWV2016399/KY).

## Compliance with ethical standards

**Conflict of interest** The authors declare that they have no conflict of interest.

## References

- Ahmad M, Rajapaksha AU, Lim JE, Zhang M, Bolan N, Mohan D, Vithanage M, Lee SS, Ok YS (2014) Biochar as a sorbent for contaminant management in soil and water: a review. *Chemosphere* 99: 19–33
- An Q, Li XQ, Nan HY, Yu Y, Jiang JN (2018) The potential adsorption mechanism of the biochars with different modification processes to Cr(VI). *Environ Sci Pollut Res Int* 25:31346–31357
- Bruun EW, Hauggaard-Nielsen H, Ibrahim N, Egsgaard H, Ambus P, Jensen PA, Dam-Johansen K (2011) Influence of fast pyrolysis temperature on biochar labile fraction and short-term carbon loss in a loamy soil. *Biomass Bioenergy* 35:1182–1189
- Burakov AE, Galunin EV, Burakova IV, Kucherova AE, Agarwal S, Tkachev AG, Gupta VK (2018) Adsorption of heavy metals on conventional and nanostructured materials for wastewater treatment purposes: a review. *Ecotoxicol Environ Saf* 148:702–712
- Cantrell KB, Hunt PG, Uchimiya M, Novak JM, Ro KS (2012) Impact of pyrolysis temperature and manure source on physicochemical characteristics of biochar. *Bioresour Technol* 107:419–428
- Chefetz B, Xing B (2009) Relative role of aliphatic and aromatic moieties as sorption domains for organic compounds: a review. *Environ Sci Technol* 43:1680–1688
- Chow JC, Watson JG, Chen L, Arnott WP, Moosmuller H, Fung K (2004) Equivalence of elemental carbon by thermal/optical reflectance and transmittance with different temperature protocols. *Environ Sci Technol* 38:4414–4422
- Deng Y, Huang S, Laird DA, Wang X, Dong C (2018) Quantitative mechanisms of cadmium adsorption on rice straw- and swine manure-derived biochars. *Environ Sci Pollut Res* 25:32418–32432
- Essandoh M, Kunwar B, Pittman CU Jr, Mohan D, Mlsna T (2015) Sorptive removal of salicylic acid and ibuprofen from aqueous solutions using pine wood fast pyrolysis biochar. *Chem Eng J* 265:219–227
- Fan Z, Zhang Q, Li M, Niu D, Sang W, Verpoort F (2018) Investigating the sorption behavior of cadmium from aqueous solution by potassium permanganate-modified biochar: quantify mechanism and evaluate the modification method. *Environ Sci Pollut Res* 25: 8330–8339
- Fan Z, Zhang Q, Gao B, Li M, Liu C, Qiu Y (2019) Removal of hexavalent chromium by biochar supported nZVI composite: batch and fixed-bed column evaluations, mechanisms, and secondary contamination prevention. *Chemosphere* 217:85–94
- Fang C, Zhang T, Li P, Jiang R, Wang Y (2014) Application of magnesium modified corn biochar for phosphorus removal and recovery from swine wastewater. *Int J Environ Res Public Health* 11:9217–9237
- Fu Y, Yang J, Cunningham AB, Towns AM, Zhang Y, Yang H, Li J, Yang X (2018) A billion cups: the diversity, traditional uses, safety issues and potential of Chinese herbal teas. *J Ethnopharmacol* 222:217–228
- Gan C, Liu Y, Tan X, Wang S, Zeng G, Zheng B, Li T, Jiang Z, Liu W (2015) Effect of porous zinc-biochar nanocomposites on Cr(VI) adsorption from aqueous solution. *RSC Adv* 5:35107–35115
- Han L, Sun K, Jin J, Wei X, Xia X, Wu F, Gao B, Xing B (2014) Role of structure and microporosity in phenanthrene sorption by natural and engineered organic matter. *Environ Sci Technol* 48:11227–11234
- Hu X, Ding Z, Zimmerman AR, Wang S, Gao B (2015) Batch and column sorption of arsenic onto iron-impregnated biochar synthesized through hydrolysis. *Water Res* 68:206–216
- Inyang MI, Gao B, Yao Y, Xue Y, Zimmerman A, Mosa A, Pullammanappallil P, Ok YS, Cao X (2016) A review of biochar as a low-cost adsorbent for aqueous heavy metal removal. *Crit Rev Environ Sci Technol* 46:406–433
- Keilweit M, Nico PS, Johnson MG, Kleber M (2010) Dynamic molecular structure of plant biomass-derived black carbon (biochar). *Environ Sci Technol* 44:1247–1253

- Kelly-Vargas K, Cerro-Lopez M, Reyna-Tellez S, Bandala ER, Luis Sanchez-Salas J (2012) Biosorption of heavy metals in polluted water, using different waste fruit cortex. *Phys Chem Earth* 37–39: 26–29
- Kim N, Park M, Park D (2015) A new efficient forest biowaste as biosorbent for removal of cationic heavy metals. *Bioresour Technol* 175:629–632
- Kyzas GZ, Kostoglou M (2014) Green adsorbents for wastewaters: a critical review. *Materials* 7:333–364
- Lee Y, Eum P, Ryu C, Park Y, Jung J, Hyun S (2013) Characteristics of biochar produced from slow pyrolysis of *Geodae-Uksae* 1. *Bioresour Technol* 130:345–350
- Li M, Liu Q, Guo L, Zhang Y, Lou Z, Wang Y, Qian G (2013) Cu(II) removal from aqueous solution by *Spartina alterniflora* derived biochar. *Bioresour Technol* 141:83–88
- Li J, Cao L, Yuan Y, Wang R, Wen Y, Man J (2018a) Comparative study for microcystin-LR sorption onto biochars produced from various plant- and animal-wastes at different pyrolysis temperatures: influencing mechanisms of biochar properties. *Bioresour Technol* 247:794–803
- Li Y, Tsend N, Li T, Liu H, Yang R, Gai X, Wang H, Shan S (2018b) Microwave assisted hydrothermal preparation of rice straw hydrochars for adsorption of organics and heavy metals. *Bioresour Technol* 273:136–143. <https://doi.org/10.1016/j.biortech.2018.10.056>
- Liu R, Zhao J, He K, Zhang X, Chang L, Xiang G (2018) Determination of Eupatilin in *Folium artemisiae Argyi* and its inhibitory effect on hepatoma cells. *Pharmacogn Mag* 14:129–133
- Lu H, Zhang W, Yang Y, Huang X, Wang S, Qiu R (2012) Relative distribution of Pb<sup>2+</sup> sorption mechanisms by sludge-derived biochar. *Water Res* 46:854–862
- Meng J, Feng X, Dai Z, Liu X, Wu J, Xu J (2014) Adsorption characteristics of Cu(II) from aqueous solution onto biochar derived from swine manure. *Environ Sci Pollut Res* 21:7035–7046
- Mohan D, Sarswat A, Ok YS, Pittman CU Jr (2014) Organic and inorganic contaminants removal from water with biochar, a renewable, low cost and sustainable adsorbent—a critical review. *Bioresour Technol* 160:191–202
- Nethaji S, Sivasamy A, Mandal AB (2013) Preparation and characterization of corn cob activated carbon coated with nano-sized magnetite particles for the removal of Cr(VI). *Bioresour Technol* 134:94–100
- Oliveira FR, Patel AK, Jaisi DP, Adhikari S, Lu H, Khanal SK (2017) Environmental application of biochar: current status and perspectives. *Bioresour Technol* 246:110–122
- Park J, Ok YS, Kim S, Cho J, Heo J, Delaune RD, Seo D (2016) Competitive adsorption of heavy metals onto sesame straw biochar in aqueous solutions. *Chemosphere* 142:77–83
- Peng P, Lang Y, Wang X (2016) Adsorption behavior and mechanism of pentachlorophenol on reed biochars: pH effect, pyrolysis temperature, hydrochloric acid treatment and isotherms. *Ecol Eng* 90:225–233
- Rao A, Bankar A, Kumar AR, Gosavi S, Zinjarde S (2013) Removal of hexavalent chromium ions by *Yarrowia lipolytica* cells modified with phyto-inspired Fe-0/Fe<sub>3</sub>O<sub>4</sub> nanoparticles. *J Contam Hydrol* 146:63–73
- Rizwan M, Ali S, Qayyum MF, Ibrahim M, Zia-ur-Rehman M, Abbas T, Ok YS (2016) Mechanisms of biochar-mediated alleviation of toxicity of trace elements in plants: a critical review. *Environ Sci Pollut Res* 23:2230–2248
- Saber M, Takahashi F, Yoshikawa K (2018) Characterization and application of microalgae hydrochar as a low-cost adsorbent for Cu(II) ion removal from aqueous solutions. *Environ Sci Pollut Res* 25: 32721–32734
- Shen Y, Wang S, Tzou Y, Yan Y, Kuan W (2012) Removal of hexavalent Cr by coconut coir and derived chars—the effect of surface functionality. *Bioresour Technol* 104:165–172
- Thines KR, Abdullah EC, Mubarak NM, Ruthiraan M (2017) Synthesis of magnetic biochar from agricultural waste biomass to enhancing route for waste water and polymer application: a review. *Renew Sust Energy Rev* 67:257–276
- Tripathi M, Sahu JN, Ganesan P (2016) Effect of process parameters on production of biochar from biomass waste through pyrolysis: a review. *Renew Sust Energy Rev* 55:467–481
- Uchimiya M, Wartelle LH, Klasson KT, Fortier CA, Lima IM (2011) Influence of pyrolysis temperature on biochar property and function as a heavy metal sorbent in soil. *J Agric Food Chem* 59:2501–2510
- Wang W, Li M, Zeng Q (2012) Column adsorption of chromium(VI) by strong alkaline anion-exchange fiber. *J Appl Polym Sci* 126:1733–1738
- Wang H, Gao B, Wang S, Fang J, Xue Y, Yang K (2015) Removal of Pb(II), Cu(II), and Cd(II) from aqueous solutions by biochar derived from KMnO<sub>4</sub> treated hickory wood. *Bioresour Technol* 197:356–362
- Xiao Y, Xue Y, Gao F, Mosa A (2017) Sorption of heavy metal ions onto crayfish shell biochar: effect of pyrolysis temperature, pH and ionic strength. *J Taiwan Inst Chem Eng* 80:114–121
- Yan J, Xue Y, Long L, Zeng Y, Hu X (2018) Adsorptive removal of As(V) by crawfish shell biochar: batch and column tests. *Environ Sci Pollut Res* 25:34674–34683
- Yang J, Zheng X, Jin R, Han L, Ha L, Li J, Wang L, Liu P, Chu Z, Huang C, Chang H, Lao L, Zhao B (2016) Effect of moxa smoke produced during combustion of *Aiye* (*Folium Artemisiae Argyi*) on behavioral changes in mice inhaling the smoke. *J Tradit Chin Med* 36:805–811
- Yao Y, Gao B, Inyang M, Zimmerman AR, Cao X, Pullammanappallil P, Yang L (2011) Removal of phosphate from aqueous solution by biochar derived from anaerobically digested sugar beet tailings. *J Hazard Mater* 190:501–507
- Yu KL, Lau BF, Show PL, Ong HC, Ling TC, Chen W, Ng EP, Chang J (2017) Recent developments on algal biochar production and characterization. *Bioresour Technol* 246:2–11
- Zhang L, Lv J, Chen H, Yan X, Duan J (2013) Chemical constituents from *Artemisia argyi* and their chemotaxonomic significance. *Biochem Syst Ecol* 50:455–458
- Zhang X, Gao B, Creamer AE, Cao C, Li Y (2017) Adsorption of VOCs onto engineered carbon materials: a review. *J Hazard Mater* 338: 102–123
- Zhang W, Deng Q, He Q, Song J, Zhang S, Wang H, Zhou J, Zhang H (2018a) A facile synthesis of core-shell/bead-like poly(vinyl alcohol)/alginate@PAM with good adsorption capacity, high adaptability and stability towards Cu(II) removal. *Chem Eng J* 351:462–472
- Zhang W, Zhang S, Wang J, Wang M, He Q, Song J, Wang H, Zhou J (2018b) Hybrid functionalized chitosan-Al<sub>2</sub>O<sub>3</sub>@SiO<sub>2</sub> composite for enhanced Cr(VI) adsorption. *Chemosphere* 203:188–198
- Zhang X, Lv L, Qin Y, Xu M, Jia X, Chen Z (2018c) Removal of aqueous Cr(VI) by a magnetic biochar derived from *Melia azedarach* wood. *Bioresour Technol* 256:1–10
- Zhao B, O'Connor D, Zhang J, Peng T, Shen Z, Tsang DCW, Hou D (2018a) Effect of pyrolysis temperature, heating rate, and residence time on rapeseed stem derived biochar. *J Clean Prod* 174:977–987
- Zhao G, Huang X, Tang Z, Huang Q, Niu F, Wang X (2018b) Polymer-based nanocomposites for heavy metal ions removal from aqueous solution: a review. *Polym Chem-UK* 9:3562–3582
- Zhou Q, Liao B, Lin L, Qiu W, Song Z (2018) Adsorption of Cu(II) and Cd(II) from aqueous solutions by ferromanganese binary oxide-biochar composites. *Sci Total Environ* 615:115–122

**Publisher's note** Springer Nature remains neutral with regard to jurisdictional claims in published maps and institutional affiliations.